A modal beamformer for circular arrays of 1-dimensional particle velocity sensors

Berke M. Gur

Citation: Proc. Mtgs. Acoust. **30**, 055016 (2017); doi: 10.1121/2.0000820
View online: https://doi.org/10.1121/2.0000820
View Table of Contents: http://asa.scitation.org/toc/pma/30/1
Published by the Acoustical Society of America

Proceedings of Meetings on Acoustics

Volume 30 http://acousticalsociety.org/

Acoustics `17 Boston

173rd Meeting of Acoustical Society of America and 8th Forum Acusticum
Boston, Massachusetts
25-29 June 2017

Signal Processing: Paper 3aSP2

A modal beamformer for circular arrays of 1-dimensional particle velocity sensors

Berke M. Gur
Mechatronics Engineering Department, Bahcesehir University, Istanbul, 34349, TURKEY; berke.gur@eng.bau.edu.tr

Particle velocity sensors are directional receivers that measure the particle motion associated with an acoustic wave rather than the scalar pressure that is obtained by omni-directional pressure sensors. Therefore, arrays of velocity sensors possess some desirable directional properties compared to conventional arrays of pressure sensors. In this paper, a modal beamformer for circular arrays of radially oriented 1-D acoustic velocity sensors is presented. It is shown that the highly directional modes of the acoustic field can be extracted from the sensor measurements using the spatial Fourier transform. These modes are weighted and combined to form narrow and steerable beams. The highest order of mode that can be extracted is limited by the number of vector sensors utilized in the array. Theoretical analysis and numerical simulations indicate that the proposed modal beamformer attains the same directivity performance as that of circular pressure sensor array beamformers but outperforms them in terms of white noise gain. The proposed method is validated through in-air experiments conducted in a recording studio. The circular velocity sensor array modal beamformer is suitable for low frequency in-air and underwater passive array applications.

Published by the Acoustical Society of America

 https://doi.org/10.1121/2.0000820
Proceedings of Meetings on Acoustics, Vol. 30, 055016 (2018)

1. INTRODUCTION

A vector sensor is a directional sensor that includes a conventional pressure sensor measuring the scalar pressure field and a particle motion sensor capable of measuring the vectorial particle acceleration[1] or alternatively the particle velocity fields.[2] Combining the particle motion measurements with pressure, it is possible to estimate the intensity of the acoustic field, which in turn is related to the direction of the net acoustic energy propagation. Hence, an array of vector sensors can provide a wealth of information regarding the acoustic field compared to conventional acoustic arrays that consist only of omni-directional pressure sensors.

Modal beamforming, on the other hand, is based on the decomposition of the acoustic field into it's so-called 'modes' and utilizing these modes for developing compact and highly directional acoustic arrays.[3] Although initially developed for pressure sensor arrays,[6] modal beamformers have recently been applied to linear[4] and rectangular[5] vector sensor arrays as well. In addition, a modal beamformer for small circular arrays of vector sensors was proposed by Zou and Nehorai.[7] Zou's beamformer relies on two-dimensional (2-D) velocity sensors capable of making collocated measurements of the radial and circumferential particle velocity for extracting the acoustic modes and generating a steerable array response.

In this paper, a modal beamformer suited for small circular arrays of radially oriented 1-D vector sensors is presented. The proposed method differs from existing pressure and vector sensor array modal beamformers proposed in the literature both in terms of the array structure and/or implementation of the beamformer. To this end, a new set of spatial Fourier coefficients and normalization weights are derived. The performance of the proposed beamformer is evaluated in terms of directivity and white noise gain. Finally, the directivity performance of the beamformer is validated though experiments conducted with a small six sensor array in a recording studio.

2. THEORETICAL DEVELOPMENT

In this section, the theoretical foundations of modal beamforming for circular arrays are presented. First, the acoustic field along a circular aperture is defined. This is followed by the introduction of the signal processing associated with the proposed modal beamformer for a circular array of 1-D vector sensors.

A. THE ACOUSTIC FIELD

Consider a uniform circular array of radius a and composed of M 1-D particle velocity sensors as shown in Fig. 1. The velocity sensors are arranged such that they measure the radial component of the particle velocity field. Assume that an acoustic time harmonic pressure wave with an amplitude of $\mathcal{P}$ and an angular frequency $\omega = kc$ (where k is the wavenumber and c is the speed of sound) is incident at an azimuth angle ψ_0 and an elevation angle θ_0. The azimuth angle is measured from the positive x-axis in the counterclockwise direction and the elevation angle is measured from the x-y plane with the positive sense towards the positive z-axis.

The pressure field at any point $\mathbf{r} = [r = a, \psi, \theta = 0]^T$ along the aperture is given as

$$p(\mathbf{r}) = \mathcal{P} \exp[ika \cos\theta_0 \cos(\psi - \psi_0)] \tag{1}$$

where the imaginary number is $i = \sqrt{-1}$. It should be noted that the time-harmonic term $\exp(i\omega t)$ is omitted in Eq. (1) for clarity. The expansion of the pressure field given in Eq. (1) using the Jacobi-Anger identity results in

$$p(\mathbf{r}) = \mathcal{P} \sum_{n=0}^{\infty} \varepsilon_n i^n J_n(ka \cos\theta_0) \cos[n(\psi - \psi_0)] \tag{2}$$

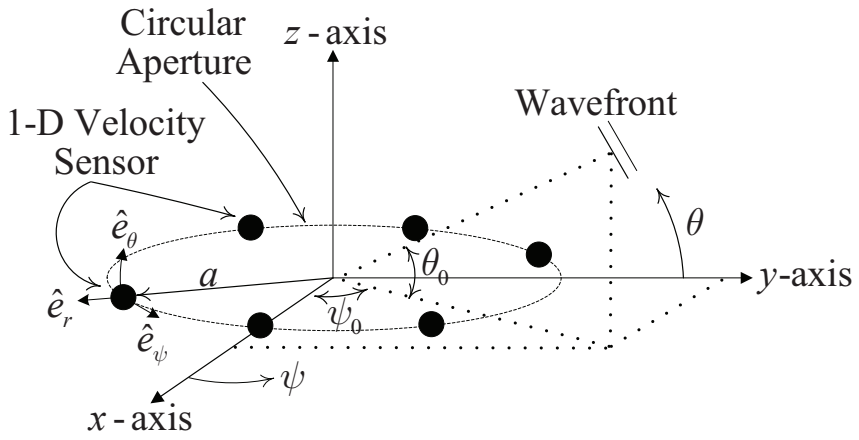

Figure 1: The small circular 1-D velocity sensor array centered at the origin of a Cartesian coordinate system and the incoming plane wave.

with $J_n(\cdot)$ being the Bessel function of the first kind, $\varepsilon_n = 1$ for $n = 0$ and $\varepsilon_n = 2$ otherwise. The Euler equation relates the particle velocity to the acoustic pressure through

$$\rho \frac{\partial}{\partial t} \vec{v}(\mathbf{r}) = -\vec{\nabla} \cdot p(\mathbf{r}) \tag{3}$$

with ρ being the ambient mass density. The gradient operator in spherical coordinates is defined as

$$\vec{\nabla} = \frac{\partial}{\partial r}\hat{e}_r + \frac{1}{r\cos\theta}\frac{\partial}{\partial \psi}\hat{e}_\psi + \frac{1}{r}\frac{\partial}{\partial \theta}\hat{e}_\theta. \tag{4}$$

In Eq. (4) $\hat{e}_r$, $\hat{e}_\psi$, and $\hat{e}_\theta$ are the radial, azimuthal, and elevational direction unit vectors, respectively (see Fig. 1). Combining Eq.'s (2)-(4), one obtains the radial component of the particle velocity at sensor m as

$$v_{r,m} = -\mathcal{V}\cos\theta_0 \cdot \sum_{n=0}^{\infty} \varepsilon_n i^{n+1} J_n'(ka\cos\theta_0)\cos[n(\psi_m - \psi_0)] \tag{5}$$

where $m = 0, 1, \ldots, M-1$ are the sensor indices and $\psi_m = 2\pi m/M$ is the azimuthal angle corresponding to sensor m. In Eq. (5) the coefficient $\mathcal{V} = -\mathcal{P}/Z$ (where $Z = \rho c$ is the characteristic impedance) is the particle velocity amplitude of the incoming wave and $J_n'(\cdot)$ is the derivative of the Bessel function with respect to its argument. This derivative of the Bessel function is computed as

$$J_n'(z) = \frac{1}{2}\left[J_{n-1}(z) - J_{n+1}(z)\right]. \tag{6}$$

B. MODAL BEAMFORMING FOR CIRCULAR ARRAYS OF 1-D VELOCITY SENSORS

The proposed modal beamformer for a circular array of 1-D velocity sensors is described in this section. Inspired by the implementation proposed by Franklin,[6] the beamformer is implemented in three steps: 1) extraction of the acoustic modes from the measurements, 2) normalization of the mode powers, and 3) combination of the modes for forming a steerable array response. The first step of extracting of the modes utilizes the spatial Fourier transform defined as

$$X(l) = \sum_{m=0}^{M-1} x_m \exp(i2\pi ml/M) \tag{7}$$

where $l = 0, 1, \ldots, M-1$ are the discrete spatial frequency indices. Applying the spatial Fourier transform given in Eq. (7) to the radial particle velocity measurements expressed in Eq. (5), one obtains the positive frequency Fourier coefficients in the form of

$$V_r(l) \approx -\mathcal{V} i^{l+1} \cos\theta_0 J_l'(ka\cos\theta_0) M \exp(-il\psi_0), \tag{8}$$

for $l = 0, 1, \ldots, L$, which are the radial particle velocity acoustic modes of the field. The negative frequencies $l = L+1, L+2, \ldots, M-1$ are dropped as they do not carry any additional information. The highest Fourier coefficient index L is defined as $L = (M-1)/2$ when M is odd and $L = M/2 - 1$ when M is even. The derivation of Eq. (8) is omitted due to space constraints. However, it should be noted that for the approximate equality to hold in Eq. (8), the aperture should satisfy the condition $ka \leq 1$. This condition leads to the upper frequency bound of $f_{\text{max}} \leq c/(2\pi a)$ for an array with a radius of a.

The higher modes of the acoustic field have lower energy. As a second step, the resulting Fourier coefficients are normalized using the weights

$$\alpha_r(l) = -[i^{l+1} J_l'(ka) M]^{-1} \tag{9}$$

The cosine and sine modes of the velocity field can be extracted by taking the real and imaginary parts of the spatial Fourier coefficients as

$$\text{Re}[\alpha_r(l)V(l)] = \mathcal{V}\cos\theta_0 \frac{J_l'(ka\cos\theta_0)}{J_l'(ka)} \cos(l\psi_0) \tag{10a}$$

$$\text{Im}[\alpha_r(l)V(l)] = -\mathcal{V}\cos\theta_0 \frac{J_l'(ka\cos\theta_0)}{J_l'(ka)} \sin(l\psi_0) \tag{10b}$$

for $l = 0, 1, \ldots, L$. The directivity of these modes increases with increasing mode order. It should be noted that unless the elevation angle of incidence θ_0 known a priori, it cannot be included in the normalization terms defined in Eq. (10).

As a final step, the modal array response is obtained by weighting the real and imaginary parts of the normalized velocity spatial frequency coefficients given in Eq. (10) by the corresponding real and imaginary filters defined as

$$\mathbf{w}_R = [\tilde{w}_0, \tilde{w}_1 \cos\psi_s, \ldots, \tilde{w}_L \cos(L\psi_s)] \tag{11a}$$

$$\mathbf{w}_I = [0, -\tilde{w}_1 \sin\psi_s, \ldots, -\tilde{w}_L \sin(L\psi_s)] \tag{11b}$$

where ψ_s is the desired steer azimuth angle, and $\tilde{w}_l$ for $l = 0, 1, \ldots, L$ are the relative weights of each mode. A factor of $\sum_{l=0}^{L} \tilde{w}_l$ is added to normalize the array response to unity when the array is steered in the direction of incidence. Relative to a reference pressure sensor located at the center of the array whose measurements are normalized to the velocity amplitude [*i.e.*, $\mathcal{V} = \mathcal{P}/Z$], the array response becomes

$$R(\psi_s) = \frac{\sum_{l=0}^{L} \left\{ \tilde{w}_l \frac{J_l(ka\cos\theta_0)}{J_l(ka)} \cos[l(\psi_s - \psi_0)] \right\}}{\sum_{l=0}^{L} \tilde{w}_l}. \tag{12}$$

If the elevation angle of incidence is close to zero ($\theta_0 = 0$; *i.e.*, the acoustic field is 2-D), the ratio $J_l(ka\cos\theta_0)/J_l(ka)$ approaches to unity. The resulting normalized beamformer response becomes

$$R(\psi_s) = \frac{\sum_{l=0}^{L} \tilde{w}_l \cos[l(\psi_s - \psi_0)]}{\sum_{l=0}^{L} \tilde{w}_l} \tag{13}$$

Typical beampatterns that are obtained for the modal beamformer described in this section, steered to $\psi_s = 50°$ for different number of sensors M and a 1 kHz airborne time-harmanic plane wave is shown in Fig. 2. The modal array radius is taken as $a = 57.5$ mm which yields a ka value of 1.06 (note that the upper theoretical frequency limit for this array is $f_{\text{max}} = 940$ Hz).

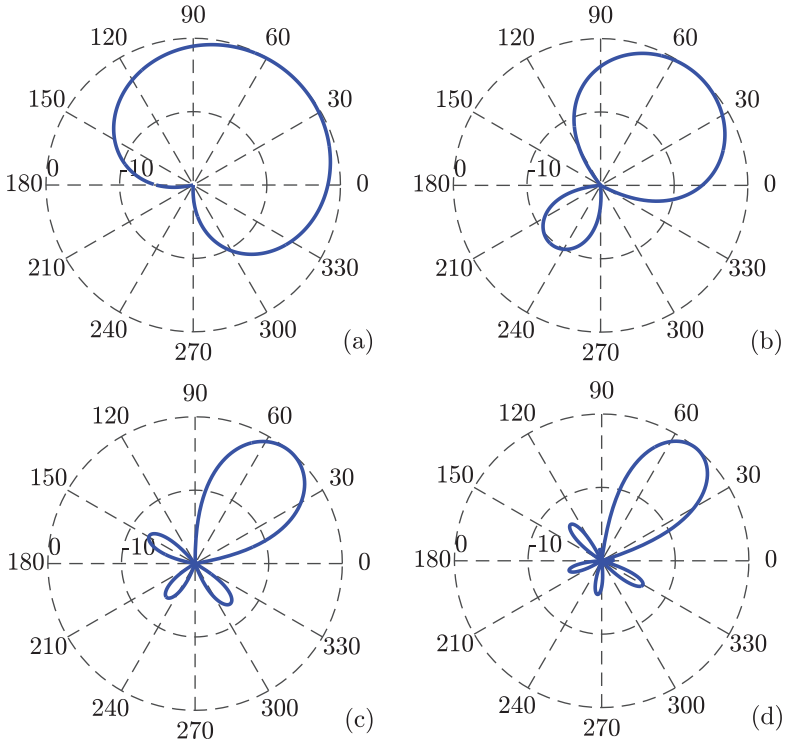

Figure 2: The beampatterns of a circular modal beamformer for an array of size $ka \approx 1$ ***and a)*** $M = 3$***, b)*** $M = 6$***, c)*** $M = 9$***, and d)*** $M = 12$ ***sensors.***

3. PERFORMANCE ANALYSIS

The most important performance metric of an array is the improvement it provides in terms of signal-to-noise ratio (SNR), which is quantified as the array gain (AG). In this section, two factors that affect the AG of the modal beamformers, namely the directivity index (DI) and white noise gain (WNG) are evaluated.[8]

A. DIRECTIVITY

The directivity of an array is expressed in terms of its directivity factor (DF) which is defined as the improvement in SNR resulting from the beamformer relative to a single omni-directional pressure sensor. More specifically, the DF is expressed as

$$\mathrm{DF} = \frac{\int_0^{2\pi}\int_{-\pi/2}^{\pi/2} F(\psi,\theta)\cos\theta d\theta d\psi}{\int_0^{2\pi}\int_{-\pi/2}^{\pi/2} B(\psi,\theta)F(\psi,\theta)\cos\theta d\theta d\psi} \tag{14}$$

where $F(\psi,\theta)$ is the intensity (*i.e.*, signal power) directivity of the noise field and $B(\psi,\theta) = |R(\psi,\theta)|^2$ is the response power or beampattern of the array. Under the assumption that the array and reference omni-directional pressure sensor responses are normalized to unity for the target signal, the numerator and denominator in Eq. (14) represent the noise power gain for the reference sensor and the array, respectively. More commonly, the DF is expressed logarithmically in terms of the directivity index (DI) which defined as $\mathrm{DI} = 10\log_{10}(\mathrm{DF})$.

The 2-D and 3-D isotropic noise fields are characterized by $F_{\mathrm{2D}}(\psi,\theta) = \delta(\theta)$ and $F_{\mathrm{3D}}(\psi,\theta) = 1$, respectively.[6] The response of the modal beamformers for 2-D fields are defined in Eq. (13) and for 3-D fields in Eq. (12. Substituting the response and the noise intensity directivity into Eq. (14) results in a DF of

$$\mathrm{DF}_{\mathrm{2D}} = \frac{2\pi\left(\sum_{l=0}^{L}\tilde{w}_l\right)^2}{\int_0^{2\pi}\left[\sum_{l=0}^{L}\tilde{w}_l\cos(l\psi)\right]^2 d\psi} \tag{15}$$

for a 2-D field and

$$\mathrm{DF}_{\mathrm{3D}} = \frac{4\pi\left(\sum_{l=0}^{L}\tilde{w}_l\right)^2}{\int_0^{2\pi}d\psi\int_{-\pi/2}^{\pi/2}\left[\sum_{l=0}^{L}\tilde{w}_l\frac{J_l(ka\cos\theta)}{J_l(ka)}\cos(l\psi)\right]^2\cos\theta d\theta} \tag{16}$$

for a 3-D field.

Another important factor that needs to be considered is the mode weights $\tilde{w}_l$. The most basic approach is to use uniform weights such as $\tilde{w}_l = 1$. For 2-D isotropic noise, it can be shown that uniform weighting results in a directivity of $\mathrm{DF}_{\mathrm{2D,unif}} = 2(L+1)^2/(L+2)$. In contrast, the DF for for 3-D isotropic noise reduces to

$$\mathrm{DF}_{\mathrm{3D,unif}} = \frac{4(L+1)^2}{\sum_{l=0}^{L}\epsilon_l\mathcal{D}(l)} \tag{17}$$

where the constant ϵ_l is defined as $\epsilon_l = 2$ for $l = 0$ and $\epsilon_l = 1$ otherwise, and the coefficients $\mathcal{D}(l)$ are computed as

$$\mathcal{D}(l) = \sqrt{\pi}\cdot\frac{\Gamma(l+1)}{\Gamma(l+3/2)} \tag{18}$$

with $\Gamma(\cdot)$ being the gamma function.

Although uniform weighting is the most straightforward choice, it is not optimal in terms of directivity. The mode weights that maximize the DF of the array can be obtained by solving a coupled multivariate optimization problem in terms of the mode weights $\tilde{w}_l$. An alternative and computationally less demanding approach for determining the optimum mode weights is possible, provided that the noise field is isotropic in the azimuthal direction. In that case, the individual modes become uncorrelated and the optimum mode weights become equal to the individual DF of that mode. Furthermore, the maximum DF of the array can be obtained by computing the DF of each mode separately and summing these individual mode directivities. A mathematical proof based on the circulant property of the isotropic noise covariance matrix was presented by Ma *et. al.*[9] Accordingly, the optimal DF mode weights for 2-D isotropic noise are obtained as

$$\tilde{w}_{\text{2D,opt}}(l) = \begin{cases} 1 & \text{if } l = 0, \\ 2 & \text{otherwise} \end{cases}$$

which yields a directivity of $\text{DF}_{\text{2D,opt}} = 1 + 2L$. Likewise, for 3-D isotropic noise the optimal mode weights can be determined as

$$\tilde{w}_{\text{3D,opt}}(l) = \begin{cases} 1 & \text{if } l = 0, \\ 4/\mathcal{D}(l) & \text{otherwise,} \end{cases}$$

yielding a maximum directivity of

$$\text{DF}_{\text{3D,opt}} = 1 + \sum_{l=1}^{L} \frac{4}{\mathcal{D}(l)} \tag{19}$$

The uniform and optimum weighted directivity results are shown in Fig. 3-a for 2-D and 3-D noise fields. The effect of optimum weighting is negligible for 2-D noise whereas improvements of up to 1.5 dB's is possible in 3-D isotropic noise fields for the same array configuration.

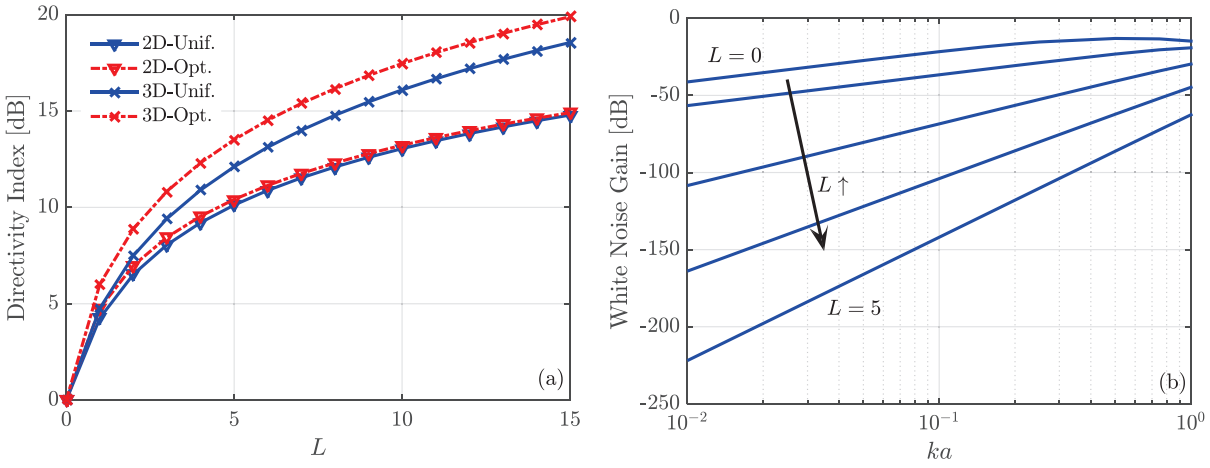

Figure 3: The performance metrics associated with the proposed modal beamformer: a) The directivity index as a function of the maximum mode order (L) for different mode weights and noise field types, and b) WNG performance for various ka values.

B. WHITE NOISE GAIN

Another type of noise that affects array performance is spatially uncorrelated noise. Such noise can be induced by local flow around the sensors and sensor electronics (electrical and thermal). The sensitivity of the array to spatially uncorrelated noise can be quantified using the white noise gain (WNG) measure, which is defined as DF in the presence of spatially uncorrelated noise. Recalling the assumption that the array response is normalized to unity in the steer direction, WNG is defined as

$$\text{WNG} = \frac{1}{\bar{\mathbf{w}}^H \bar{\mathbf{w}}} \tag{20}$$

where $\bar{\mathbf{w}}$ is the weight applied to the measurements (includes Fourier transformation operations, normalization terms, and steering filter coefficients) and the superscript $(\cdot)^H$ denotes the Hermitian operator. As with the DF, a higher WNG is better in terms of array performance. The numerically computed WNG values are plotted in Fig. 3-b as a function of ka for different mode orders (L) for the proposed velocity modal beamformer. The WNG performance of modal beamformer is poor, in particular, at low frequencies. Hence, as pointed by Guo *et. al.*,[8] there exists a trade-off between directivity and white noise performance; as the number of modes included in the beamformer increases, directivity improves at the cost of WNG.

4. EXPERIMENTAL VALIDATION

PU mini type acoustic vector sensor (AVS) developed by Microflown Technologies are used in the circular velocity sensor array constructed for experimentally evaluating the proposed beamformer. The PU mini sensor is based on the principle of anemometry and combines a low-cost pressure sensor (represented by the 'P' in PU) and a 1-D velocity sensor (represented by the 'U' in PU) and in a single compact package.[2] Although both magnitude and phase calibration data are provided with the sensors by Microflown, this data was not available for the specific sensors used in the experiments, necessitating their recalibration.

A. THE CALIBRATION SETUP

For the calibration of the velocity sensor, a rigid walled, long standing wave tube (SWT) is designed and manufactured. The tube is made from stainless steel with an inner diameter of $d_i = 52$ mm and a thickness of 4 mm. The length of the tube is 740 mm with a measurement position opened at $\xi = 220$ mm from the termination cap for the particle velocity sensor. Flanges are welded to the two opposite ends of the tube and serve as mounting points for the acoustic source and reference microphone. The cut-off frequency (i.e., the highest frequency for which standing waves are formed in the tube) for this SWT is determined to be approximately $f_c = c/(1.7d_i) \approx 4$ kHz. To prevent acoustic energy leakage (*e.g.*, from sensor mountings) at low frequencies (< 100 Hz), rubber O-rings are used for achieving airtight connections. A single Sammi NSU-75B compression driver is used as an acoustic source. The reference microphone is of model PCB type 130E22 IEPE array microphone is placed at the rigid termination facing the source at the other end of the SWT. This microphone has a sensitivity of 37 mV/Pa at 1 kHz (with a variation within ± 1 dB for 100 Hz to 10 kHz). Digitization of the acquired sensor data is performed at a sampling rate of 6.4 kHz using a National Instruments cDAQ-9178 platform that employs 24 bit sigma-delta analog-to-digital converters (ADC). No filtering except for hardware based anti-aliasing filtering is performed. The complete SWT setup used for the calibration of the vector sensors is shown in Fig. 4.

B. CALIBRATION OF THE VELOCITY SENSORS

The Microflown 1-D particle velocity sensors are calibrated based on the theoretical particle velocity frequency response function (FRF) defined as $H^{\text{th}}_{p\text{-}v}(f) = V(f)/P_{\text{ref}}(f) = (i/Z)\sin(2\pi f\xi/c)$ relative to the reference microphone inside the SWT. The theoretical FRF is compared with the experimental estimates of the FRF defined as $H^{\text{exp}}_{p\text{-}v}(f) = P_{xy}(f)/P_{xx}(f)$, where P_{xx} is the auto-power spectral density of the reference microphone, and P_{xy} is the cross power spectral density between the reference and the velocity sensor. A 1024 point FFT and 50% overlapping Hanning window is used to compute the spectral densities from the measurements. Following the procedure suggested by the sensor manufacturer, parametric correction factors (CF) are defined for the velocity sensors in the form of $C_v(f) = H^{\text{th}}_{p\text{-}v}(f)/H^{\text{exp}}_{p\text{-}v}(f) = \mathcal{C}_v \exp(i\phi_v)$ where

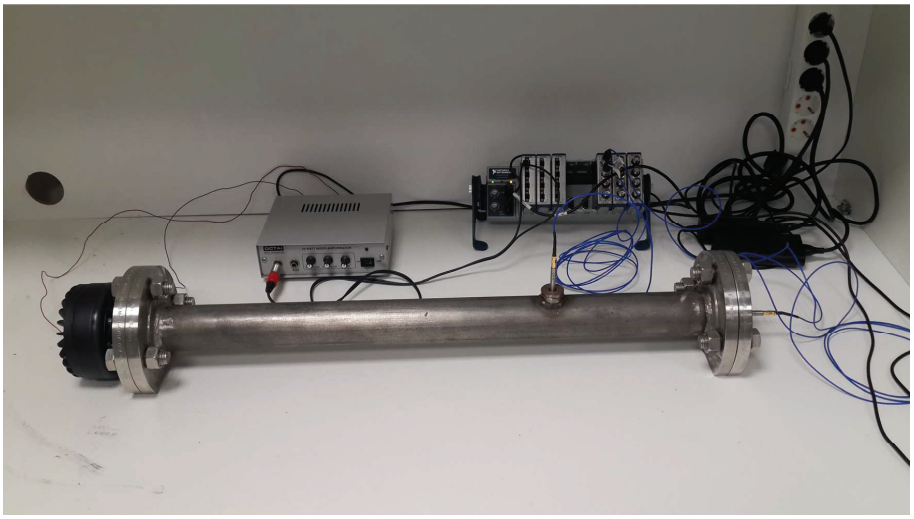

Figure 4: The SWT setup used for calibrating the AVS.

$$\mathcal{C}_v = \frac{1}{S_v} \frac{[1 + (f_{v,1}^2/f^2)]^{1/2} \cdot [1 + (f/f_{v,2}^2)]^{1/2}}{[1 + (f^2/f_{v,3}^2)]^{1/2}} \tag{21a}$$

$$\phi_v(f) = -\arctan\left(f_{v,4}/f\right) - \arctan\left(f/f_{v,5}\right) - \arctan\left(f/f_{v,6}\right), \tag{21b}$$

S_v is the velocity sensor sensitivity at 250 Hz [units mV/(mm/s)], and $f_{v,i}$ are the corner frequencies. Note that these CF's are the inverse of the sensor sensitivities. The experimental FRF's $H_{p\text{-}v}^{\text{exp}}(f)$ are curve-fit to the theoretical FRF's $H_{p\text{-}v}^{\text{th}}(f)$ through the CF's defined in Eq. (21). The curve-fitting is performed using a non-linear least-squares method based on the Levenberg-Marquardt algorithm, resulting in an estimate of the sensor sensitivities and the corner frequencies for each Microflown velocity sensor. The parameters are initialized using typical values provided by the sensor manufacturer. Representative results for the curve-fitting procedure of a single sensor are presented in Fig. 5. The sine function FRF changes sign the node points of magnitude FRF. Due to the sign change of the FRF, the phase response exhibits sudden and progressive jumps of 180° at these points. The experimentally obtained FRF's also exhibit the progressive 180° jumps in the phase response as can be seen in Fig. 5.

C. ROOM EXPERIMENTS

To validate the proposed modal beamformer, a set of broadcast experiments are conducted inside a recording studio with a small circular array of particle velocity sensors. As depicted in Fig. 6, the walls and the ceiling of the studio are covered with acoustically damped material while the floor is made of wood. An Adam Audio A7X nearfield loudspeaker is used as the source. The circular velocity sensor array (also depicted in Fig. 6, mounted on a tripod) consists of 6 radially oriented Microflown 1-D particle velocity sensors, placed uniformly along an aperture of 115 mm in diameter. The separation between the speaker and the array was two wavelengths or more. The same data acquisition hardware and setup parameters

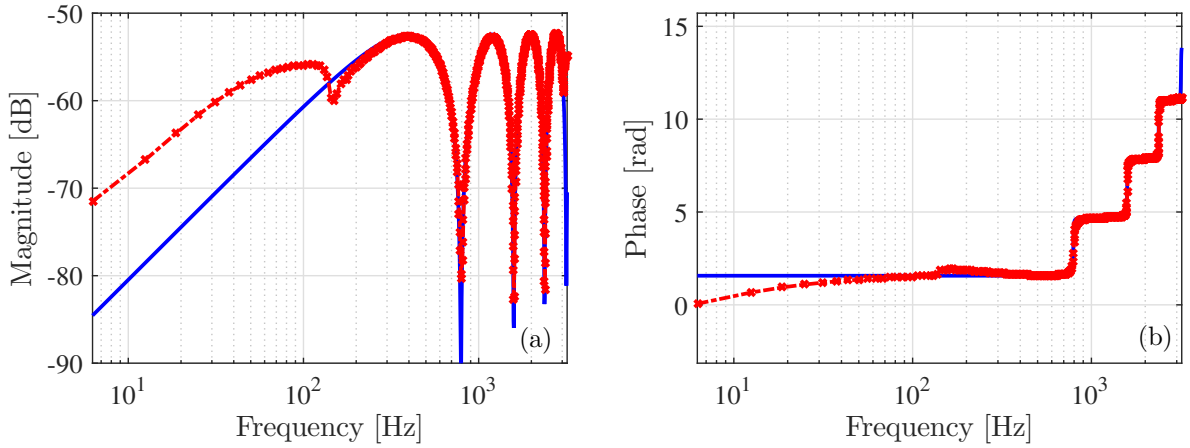

Figure 5: A set of representative results from the velocity sensor calibration experiments: a) the magnitude and b) the phase response of the theoretical (blue, solid) and experimental (red, dash-dot) FRF's for calibrated 1-D velocity sensor.

described above for the calibration of the velocity sensors are used for these room experiments as well. Narrowband, harmonic signals as well as broadband Gaussian signals were broadcast. For a given azimuthal array orientation relative to the loudspeaker (*i.e.*, the ψ_0 angle) the array was electronically steered to regularly spaced azimuthal angles and the response power was recorded, resulting in experimental beampatterns. Such typical experimental beampatterns for various arrival directions are shown in Fig. 7. These experimental results indicate a good agreement with the theoretical beampatterns. Slight shifts in the main lobe direction and grating lobes are also observed in several cases. Simulations reveal that such main lobe direction shifts and grating lobes are likely caused by errors in the orientation of the sensors which may lead to phase mismatches in the velocity measurements. Although the array rig used in the experiments allowed precise azimuthal (ψ_m) placement of the sensors, the orientation of the velocity sensors was manually set by the author, resulting in phase mismatch.

5. CONCLUSION

In this paper, a modal beamformer for small circular apertures of 1-D particle velocity sensor arrays is introduced. The proposed method computes the spatial Fourier transform of the radial particle velocity field for obtaining the acoustic modes. Although their directivity increases, the strength of the acoustic modes decreases with increasing mode order. Hence, a normalization factor is computed and applied to each mode, followed by a steering filter. The performance of the resulting beamformer is evaluated in terms of directivity in 2-D and 3-D isotropic fields as well as white noise gain. Directivity predictions for both uniform weighting and optimal directivity weighting of the modes are presented. These results indicate that up to 1.5 dB directivity improvement can be achieved if optimal weighting is used in 3-D isotropic noise. Finally, the proposed beamformer is evaluated through in-air experiments conducted with an array of six 1-D velocity sensors, showing good agreement with theoretical directivity predictions. These experiments further revealed that the proposed approach is very sensitive to phase mismatch between the velocity sensors. Future work will focus on mitigating the effects of sensor mismatch on beamformer performance.

Figure 6: The recording studio and the experimental setup showing the circular array in the foreground and the speaker that is used as the acoustic source behind it.

ACKNOWLEDGMENTS

The author would like to express his sincere appreciation to the European Commission FP7 PEOPLE Marie Curie Actions Program for supporting this research (grant no: PIRG-GA-2009-256585).

REFERENCES

[1] M. T. Silvia, R. T. Richards, "A theoretical and experimental investigation of low-frequency acoustic vector sensors," in *Proc. MTS/IEEE OCEANS '02 Conf.* 1886-1897 (2002).

[2] F. Jacobsen, H. E. de Bree, "*The microflown particle velocity sensor*", in Handbook of Signal Processing in Acoustics, ed. D. Havelock, S. Kuwano, M. Vorlander. New York: Springer, 1283-1291 (2009).

[3] H. Teutsch, "Modal Array Signal Processing: Principles and Applications of Acoustic Wavefield Decomposition", Berlin Heidelberg: Springer-Verlag, 41-92 (2007).

[4] B. Gur, "Particle velocity gradient based acoustic mode beamforming for short linear vector sensor arrays", *J. Acoust. Soc. Am.* **135**(6), 3463-3473 (2014).

[5] X. Guo, S. Yang, S. Miron, "Low-frequency beamforming for a miniaturized aperture three-by-three uniform rectangular array of acoustic vector sensors", *J. Acoust. Soc. Am.* **138**(6), 3873-3883 (2015).

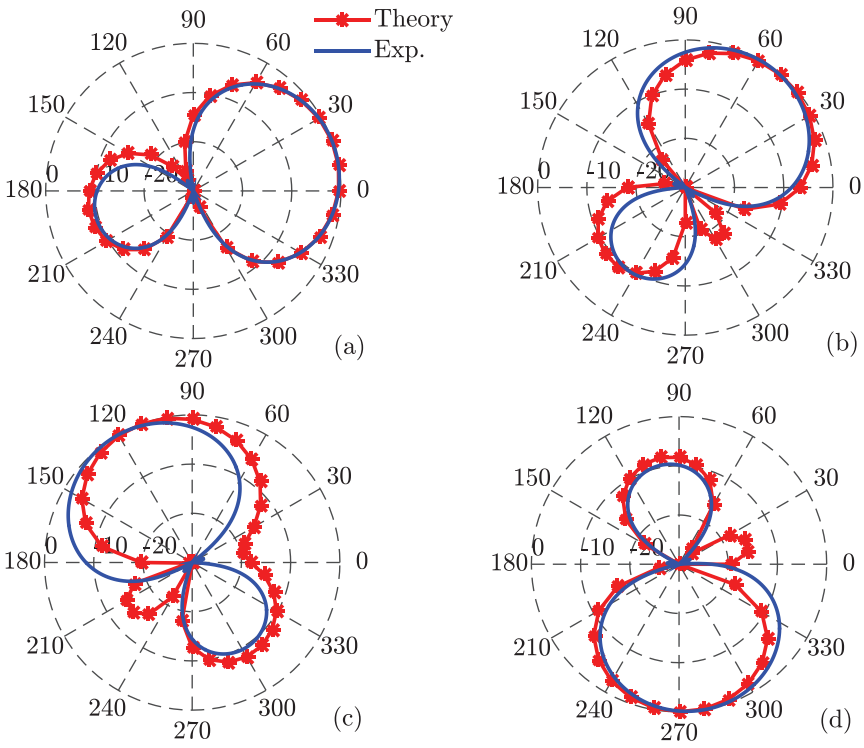

Figure 7: The theoretical (blue, solid) and experimentally obtained (red, dash-star) beampatterns associated with radial particle velocity modal beamformer of $M = 6$ ***sensors steered to a)*** $\psi_s = 15°$***, b)*** $\psi_s = 57°$***, c)*** $\psi_s = 123°$***, and d)*** $\psi_s = 279°$***. The actual steer direction was obtained from the radial vector sensor array measurements made simultaneously with the velocity array measurements.***

[6] J. B. Franklin, "Superdirective Receiving Arrays for Underwater Acoustic Application", DREA Contractor Report 97/444 P.O. Box 1012, Dartmouth, Nova Scotia, Canada, B2Y 3Z7, 44 pp. (1997).

[7] N. Zou, A. Nehorai, "Circular acoustic vector-sensor array for mode beamforming", *IEEE Trans. Signal Process.*, **57**(8), 3041-3052 (2009).

[8] X. Guo, S. Miron, Y. Yang, S. Yang, "An upper bound for the directivity index of superdirective acoustic vector sensor arrays", *J. Acoust. Soc. Am.* **140**(5), EL410 (2016).

[9] Y. Ma, Y. Yang, Z. He, K. Yang, C. Sun, and Y. Wang, "Theoretical and practical solutions for high-order superdirectivity of circular sensor arrays," IEEE Trans. Ind. Elec. **60**(1), 203-209 (2013).